Climatic Change (2014) 126:413–427
DOI 10.1007/s10584-014-1234-9

Response of evapotranspiration and water availability to the changing climate in Northern Eurasia

Yaling Liu · Qianlai Zhuang · Zhihua Pan · Diego Miralles · Nadja Tchebakova · David Kicklighter · Jiquan Chen · Andrey Sirin · Yujie He · Guangsheng Zhou · Jerry Melillo

Received: 17 October 2013 / Accepted: 17 August 2014 / Published online: 28 August 2014

Abstract Northern Eurasian ecosystems play an important role in the global climate system. Northern Eurasia (NE) has experienced dramatic climate changes during the last half of the

Electronic supplementary material The online version of this article (doi:10.1007/s10584-014-1234-9) contains supplementary material, which is available to authorized users.

Y. Liu (✉) · Q. Zhuang · Y. He
Department of Earth, Atmospheric, and Planetary Sciences, Purdue University, West Lafayette, IN, USA
e-mail: liu516@purdue.edu

Q. Zhuang
Department of Agronomy, Purdue University, West Lafayette, IN, USA

Z. Pan
College of Resources & Environmental Sciences, China Agricultural University, Beijing, China

D. Miralles
Laboratory of Hydrology and Water Management, Ghent University, Ghent, Belgium

D. Miralles
School of Geographical Sciences, University of Bristol, Bristol, UK

N. Tchebakova
V N Sukachev Institute of Forest, Siberian Branch of the Russian Academy of Sciences, Academgorodok, Krasnoyarsk, Russia

D. Kicklighter · J. Melillo
The Ecosystems Center, Marine Biological Laboratory, Woods Hole, MA, USA

J. Chen
CGCEO/Geography, Michigan State University, East Lansing, MI 48824, USA

A. Sirin
Laboratory of Peatland Forestry and Amelioration, Institute of Forest Science, Russian, Academy of Sciences, Uspenskoye, Moscow Oblast, Russia

G. Zhou
Institute of Botany, The Chinese Academy of Sciences, Beijing, China

20th century and to present. To date, how evapotranspiration (*ET*) and water availability (*P*–*ET*, P: precipitation) had changed in response to the climatic change in this region has not been well evaluated. This study uses an improved version of the Terrestrial Ecosystem Model (TEM) that explicitly considers *ET* from uplands, wetlands, water bodies and snow cover to examine temporal and spatial variations in *ET*, water availability and river discharge in NE for the period 1948–2009. The average *ET* over NE increased during the study period at a rate of 0.13 mm year^{-1} year^{-1}. Over this time, water availability augmented in the western part of the region, but decreased in the eastern part. The consideration of snow sublimation substantially improved the *ET* estimates and highlighted the importance of snow in the hydrometeorology of NE. We also find that the modified TEM estimates of water availability in NE watersheds are in good agreement with corresponding measurements of historical river discharge before 1970. However, a systematic underestimation of river discharge occurs after 1970 indicates that other water sources or dynamics not considered by the model (e.g., melting glaciers, permafrost thawing and fires) may also be important for the hydrology of the region.

1 Introduction

Evapotranspiration (*ET*) is a key component of the Earth system. It links the Earth surface energy balance with its water balance and affects the biogeochemical exchanges between the biosphere and atmosphere (Dolman and de Jeu 2010; Wang and Dickinson 2012). *ET* conveys about half of the solar energy absorbed by the land back to the atmosphere as latent heat flux (Stephens et al. 2012). Because water vapor is the dominant greenhouse gas in the atmosphere (Held and Soden 2000), *ET* is thus critical in regulating the Earth's energy balance and therefore its temperature. In addition, *ET* returns more than 60 % of annual precipitation (*P*) back to the atmosphere, constraining the water availability over the continents (Vörösmarty et al. 1998; Miralles et al. 2011a; Kumar et al. 2014), and providing climate feedbacks via precipitation recycling (Seneviratne et al. 2010).

There is a growing consensus that water availability is becoming a more crucial limiting factor for economic development (Vörösmarty et al. 2010). With an increasing human population, the rapidly rising demand for water is causing this resource to become progressively scarce. Climatic change may exacerbate this water limitation, as future warming is expected to raise the rates of *ET* and then lead to further drying of the land surface (Huntington 2006; Douville et al. 2012), particularly in regions already suffering from water scarcity (Dorigo et al. 2012).

To date, *ET* is deemed as one of the most difficult components of the hydrological cycle to quantify accurately (Dolman and De Jeu 2010), partially because a large number of environmental (e.g., soil moisture, plant phenology, soil properties) and climatic factors (e.g., solar radiation, temperature, humidity, wind speed) affect the process (e.g., Monteith 1965). Understanding historical changes in *ET* would enable a better quantification of the future availability of water across the continents, which in turn, may help to better manage water resources via irrigation scheduling, drought detection and assessment and so forth. Recently developed methodologies that up-scale in situ measurements (Jung et al. 2010; Xiao et al. 2012) or combine satellite-based data (Lu and Zhuang 2010; Fisher et al. 2008; Miralles et al. 2011a, b; Mu et al. 2011) provide new opportunities to estimate *ET* over large regions for the limited time period of observational records. These spatially explicit estimates can also be used to benchmark land surface models (Mueller et al. 2013), which in turn, can estimate changes in regional hydrology for longer time period in the past or project these changes into the future.

Ecosystems in Northern Eurasia (NE) play an important role in the global climate system due to their high sensitivity to climatic change and the vast land area that they cover (Adam and Lettenmaier 2008; Groisman et al. 2010). NE accounts for 19 % of the Earth's land surface, 59 % of the terrestrial land north of 40°N, about 70 % of the Earth's boreal forests, and more than two-thirds of the Earth's permafrost (NEESPI 2004). While it is widely accepted that the Earth's temperature has increased globally in recent decades, this increase has been more rapid in NE (Groisman et al. 2009; IPCC 2013). A significant portion of the total terrestrial freshwater flux to the Arctic Ocean is generated in this region (Frey and Smith 2003); increases in this freshwater flux may potentially weaken the North Atlantic thermohaline circulation and slow CO_2 transport to the deep ocean (Peterson et al. 2002; ACIA 2005). Despite this crucial role, little is known about how past changes in climate have affected the terrestrial water cycle in the region.

This study uses an improved version of a process-based biogeochemistry model, the Terrestrial Ecosystem Model (TEM 5.0; Zhuang et al. 2010), to gain new insights into the dynamics of the terrestrial water cycle in NE. TEM is a process-based biogeochemistry model that uses spatially referenced data on climate, soils, land cover, and elevation to simulate C, N, and water fluxes and pools in terrestrial ecosystems (e.g., Zhuang et al. 2010; Liu et al. 2013). With a long time series of forcing data, TEM estimates allow a longer-term (1948–2009) analysis of *ET* and water availability (*P–ET*) than the one based on satellite-based *ET* datasets only. The *ET* algorithms in the previous version of TEM (Zhuang et al. 2010 – hereafter referred to as TEM-AL1) do not consider the effects of land cover heterogeneity on *ET* estimation, which are particularly important when modeling *ET* and are not well addressed by many of the currently existing *ET* estimation schemes (Mengelkamp et al. 2006; Mueller et al. 2013). In addition, the atmospheric evaporative demand (AED) in TEM-AL1 is represented by the Jensen-Haise formula (Jensen and Haise 1963) and is only affected by variations in climate. This formula is reported to overestimate AED during the summer (Feddes and Lenselink 1994) so that *ET* is also overestimated by TEM-AL1 (Liu et al. 2013). To address these limitations, we developed new *ET* algorithms for TEM – hereafter referred to as TEM-AL2 – to improve the simulation of *ET* in high latitude ecosystems (see Section 2.2). In Section 2 of this study, we: (a) describe the improvements to the TEM *ET* algorithms, (b) parameterize the improved TEM using data from eddy-covariance (EC) towers, and (c) evaluate *ET* estimates from the improved TEM by comparisons against satellite-based *ET* products. Section 3 focuses on the analysis of the historical changes in *ET*, with special emphasis on the implications of these changes for the availability of water resources in NE.

2 Methods

2.1 Overview

In a recent study (Liu et al. 2013), we found that the Penman-Monteith approach incorporating physiological and aerodynamic constraints on AED provided better estimates of *ET* across the Mongolian Plateau than TEM-AL1, which is based on empirical relations of *ET* with solar radiation and air temperature described by Jensen and Haise (1963). However, in Liu et al. (2013), ET was estimated from transpiration and soil surface evaporation in only uplands (i.e. upland ecosystems). Here, we further modify the TEM *ET* algorithms to estimate: 1) transpiration separately for uplands and wetlands; 2) evaporation separately for uplands, wetlands, and water

bodies; and 3) snow sublimation. We refer to the new algorithms as TEM-AL2. These modifications aim at improving the representation of the interactions between the terrestrial energy and water budgets and to increase their realism in high-latitude regions. The different *ET* components are aggregated to grid cell scale (hereafter ET_a) weighted by the fraction of each land cover per grid cell (see Eq. 1 and 2 in Section 2.2). The fraction coverages of uplands, wetlands and water bodies are assumed to be static within each grid cell and sum to 1, but these land cover types may be totally or partially covered by snow during some part of the year. The fractional snow cover varies monthly and is represented with seasonal snow cover climatology (see Section 2.1 in the Supplementary Materials). Then regional *ET* is estimated by calculating area-weighted average of ET_a across all grid cells in NE. Finally, regional estimates of *ET* are examined for temporal trends.

To calibrate the TEM-AL2 and evaluate its performance relative to the TEM-AL1 version, *ET* measurements from 13 EC sites in the NE are used (http://www.asianflux.com, http://gaia.agraria.unitus.it/, Table S4, Fig. 1a). In addition, two satellite-based *ET* products – the MODIS product (Mu et al. 2011, hereafter MODIS-ET) and GLEAM (Global Land-surface Evaporation: the Amsterdam Methodology, Miralles et al. 2011a, b) – are also compared to EC data to evaluate their validity at the site level relative to TEM. These satellite products along with the mean of the LandFlux-EVAL merged *ET* synthesis datasets (hereafter EVAL) by Mueller et al. (2013), and the PM-Mu *ET* estimates by Vinukollu et al. (2011) are used to evaluate the spatio-temporal variability of the regional TEM-AL2 *ET* estimates in Section 2.6. EVAL and PM-Mu *ET* estimates are not compared with EC data because of differences in the timing of the *ET* estimates and the EC measurements. In this study, we use the Mann-Kendall trend test (Hamed and Rao 1998) to determine significant time-series trends.

2.2 Modification of ET algorithms

In this study, we continue our revision of TEM-AL1 based on Liu et al. (2013) by incorporating separate algorithms and parameterizations to derive monthly *ET* (or evaporation) from uplands, wetlands, water bodies and snow cover. *ET* from uplands includes transpiration from plant canopies, evaporation from wet canopies, saturated and moist soil surfaces. Although the same algorithms are used in wetlands as in uplands, *ET* is assumed to be not limited by water in wetlands (see e.g. Mohamed et al. 2012). For water bodies, evaporation is estimated based on algorithms described by Penman (1948, 1956). Snow sublimation is estimated based on algorithms described by Zhuang et al. (2002). Because we assume that any snow is uniformly distributed within a grid cell, the effects of snow dynamics on *ET* from a particular land cover type or plant function type (PFT) in a grid cell is determined as follows:

$$ET_i = (1-p_s) \times ET_{i0} + p_s \times ET_s \quad (1)$$

where ET_{i0} represents monthly *ET* from the fraction of the *ith* land cover or PFT within each grid cell not covered by snow; ET_s is snow sublimation; p_s is the fraction of a grid cell covered by snow; and ET_i is the *ET* from the *ith* land cover or PFT both covered and uncovered by snow within a grid cell. Fractional snow cover is relatively low during summer and high during winter. The total *ET* of each grid cell (ET_a) is then calculated by aggregating the *ET* estimates for both snow-free and snow-covered uplands, wetlands and water:

$$ET_a = p_u \times ET_u + p_t \times ET_t + p_w \times ET_w \quad (2)$$

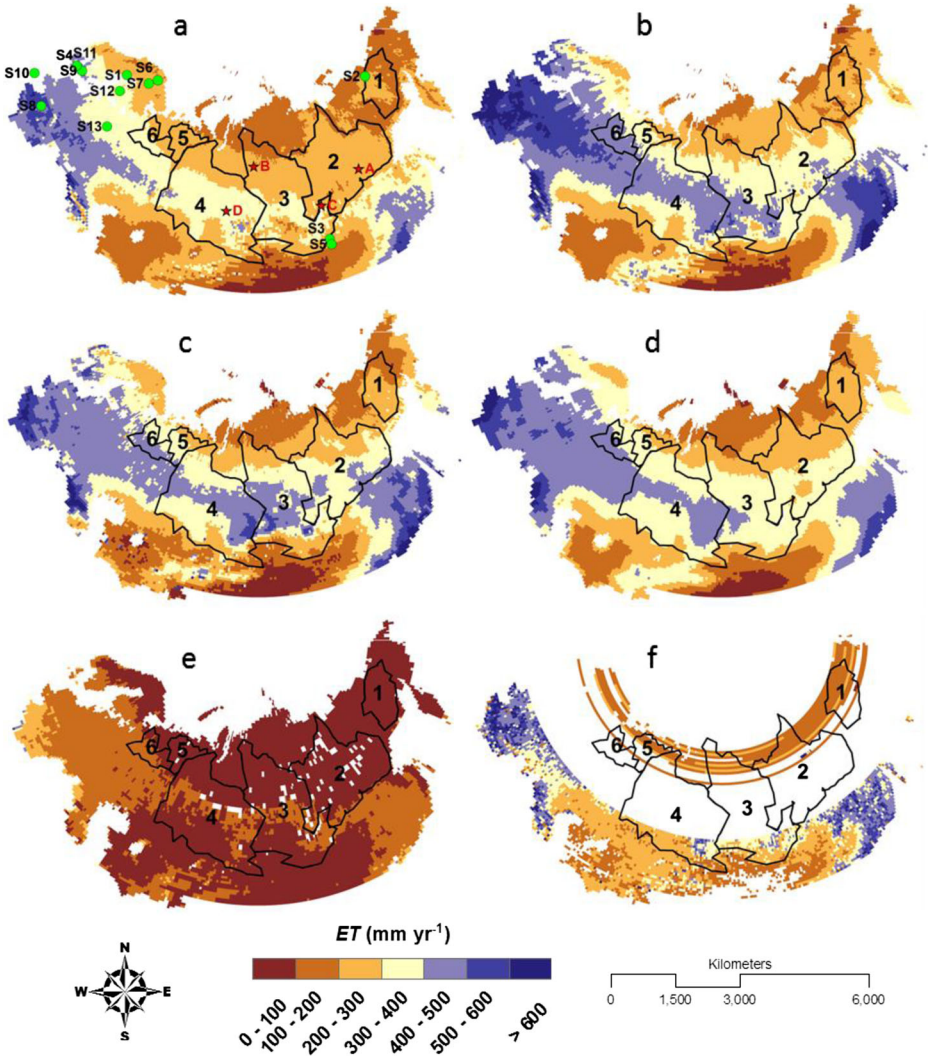

Fig. 1 Spatial patterns of average annual *ET* for uplands in the NE estimated by TEM and several satellite products: **a** TEM-AL1 *ET* during 2000–2009, **b** TEM-AL2 *ET* during 2000–2009, **c** GLEAM (Global Land-surface Evaporation: the Amsterdam Methodology) during 2000–2009, **d** the mean of LandFlux-EVAL merged synthesis product during 2000–2005, **e** PM-Mu *ET* during 2000–2007 in Vinukollu et al. (2011) and **f** MODIS-ET during 2000–2009. Areas with missing values or filled values are blanks on the map. The boundaries of six major river watersheds in the NE are delineated; 1, 2, 3, 4, 5 and 6 stand for Kolyma, Lena, Yenisei, Ob, Pechora and Northern Dvina watershed, respectively. The 13 EC sites and the four grid cells used for the simulation experiment are also shown on a), where EC site codes (S1–S13) and cell codes (A-D) correspond to those in Table S4 and Table S8 (Supplementary Materials), respectively. Note that the boundaries and numbers remain the same for all maps in this study

where p_u, p_t, and p_w represent the fractions of uplands, wetlands and water bodies within each grid cell, respectively (i.e., the sum of p_u, p_t and p_w is 1). ET_u, ET_t, and ET_w represent the ET_i (see Eq. 1) from the uplands, wetlands and water bodies for the corresponding grid cell, respectively. Information about the TEM-AL2 algorithms and the differences between the

TEM-AL1 and TEM-AL2 is provided in Section 1 and Table S1 of the Supplementary Materials.

2.3 Input data

Input data on air temperature (T), precipitation (P), cloudiness (C), vapor pressure (V), wind speed (u), atmospheric CO_2 concentrations, land cover type, albedo, elevation, and soil texture are needed to estimate ET using the TEM-AL2. Surface incoming shortwave radiation (R) is estimated from the TEM by using latitude, date, and cloudiness (Pan et al. 1996). Soil texture, elevation and land cover data vary spatially over the study region and are assumed to remain unchanged throughout 1948–2009, whereas other inputs vary over time and space. In this study, all simulations are conducted at a spatial resolution of 0.5° latitude × 0.5° longitude.

Gridded historical time series of monthly T, P, C, and V from the Climate Research Unit of the University of East Anglia (CRU TS3.10, the precipitation dataset is the corrected version v3.10.01; Harris et al. 2013) are used. The CRU dataset has been selected for this study because its accuracy stands out from a variety of widely-used forcing datasets in the NE region (Liu et al. 2013; Simmons et al. 2004; Liu et al. in review). For u we use monthly climatology data during 1961–1990 from CRU, due to the unavailability of historical time series. In addition, the spatial resolution of these wind data is degraded from 10′ to 0.5° by averaging values of 10′ cells within each 0.5° cell, to be consistent with the other forcing datasets. In Section 2.1 of the Supplementary Materials we assessed the quality of the CRU data used in this study by comparing them against observations from thousands of weather stations. An average absolute mean percentage difference (MPD) of below 16 % across all stations for each climate variable (except for C) suggests a good representation of the regional climate conditions.

For snow dynamics, we use a seasonal climatology of snow cover derived from MODIS Snow Cover monthly data (MOD10CM) from 2000 to 2012, due to unavailability of snow cover time series covering the entire period 1948–2009. Thus, our analyses do not capture the signal of warming-induced reduction of snow cover over the most recent decades (ACIA 2005). Despite this limitation, the introduction of seasonal snow coverage is an effort to increase the realism of the model representation of the NE region, where snow prevails during several months per year. Description of other ancillary data used in this study is provided in Section 2 of the Supplementary Materials.

2.4 Model parameterization

Many parameters involved in the TEM-AL2 are defined from literature values (e.g., Shuttleworth 1992; ASCE 1996; Mu et al. 2011). However, some parameters such as the relative sensitivity of soil moisture to vapor pressure deficit (β), specific leaf area (SLA), mean potential stomata conductance per unit leaf area (C_L), and coefficients for calculating the net emissivity between the atmosphere and the ground (a_e, b_e) for each PFT need to be calibrated using EC measured evaporation fluxes. For ecosystems that have more than one EC site, we conduct "leave-one-out" cross validation (Zhang 1993) to yield one set of parameter combinations by PFT.

MODIS albedo data (MCD43C3) for 2005 is used to determine the mean monthly albedo of each PFT (Jin et al. 2003a, b; Salomon et al. 2006). It is assumed that the albedo remained unchanged during 1948–2009 due to the unavailability of time series data. The monthly albedo of each PFT is then used as PFT-specific parameters.

2.5 Site-level evaluation

Comparisons of site-level estimates of *ET* from TEM-AL1 and TEM-AL2 against measured *ET* at the 13 EC sites demonstrate that the calibrated TEM-AL2 (Fig. S2) systematically outperforms the TEM-AL1 (Fig. S3). The parameterization of TEM-AL2 to latent heat flux data measured at EC sites for various PFTs allows consideration of effects of different land characteristics on AED, and subsequently *ET*, whereas TEM-AL1 considers only changes in climate conditions when estimating AED. TEM-AL2 *ET* captures the seasonality of the measured *ET* well at all sites (Fig. S2). The ratio of *ET* to precipitation (i.e., *ET*/*P*) from TEM-AL2 *ET* is very close to that measured at the EC sites (Table S4). An average root mean square difference (RMSD) of 8.54 mm mon^{-1}, Nash–Sutcliffe model efficiency coefficient (NS) of 0.81, mean percent difference (MPD) of 8.96 %, and Pearson correlation coefficient (r) of 0.95 across all sites (Table S5) indicate that the TEM-AL2 *ET* compares reasonably well with field measurements. In contrast, TEM-AL1 overestimates *ET* during summer for the majority of the locations (Fig. S3), mostly due to the overestimation of AED in summer (Liu et al. 2013). After calibration, TEM-AL2 *ET* estimates are also closer to the EC measurements than MODIS-ET (average RMSD, NS and r of 15.26 mm mon^{-1}, 0.51, and 0.90, respectively) and GLEAM (average RMSD, NS and r are 12.86 mm mon^{-1}, 0.62 and 0.91, respectively). Generally MODIS overestimates *ET* in summer relative to EC measurements (Fig. S4), while GLEAM matches the seasonal patterns of measurements well at most sites (Fig. S5) although it overestimates the *ET* during the summer at the xeric shrublands site (Ivotuk) and the tundra wetland site (SEFaj).

2.6 Evaluation of the spatiotemporal variability of ET

All of the aforementioned satellite-based products (MODIS-ET, GLEAM, EVAL, PM-Mu *ET*), TEM-AL1 and TEM-AL2 report *ET* estimates for upland ecosystems, whereas only TEM-AL2 and GLEAM account for *ET* (or evaporation) from snow, water bodies and wetlands. For consistency, we use the TEM-AL2 *ET* estimates for only upland ecosystems in the assessment of their spatial distribution by comparison to TEM-AL1 *ET* and the above mentioned satellite products.

Overall, the average *ET* estimated by TEM-AL2 for NE is 270.1 mm $year^{-1}$ during 2000–2009, slightly lower than the 298.5 mm $year^{-1}$ estimated by GLEAM and the 303.3 mm $year^{-1}$ estimated by EVAL, and much lower than the 341.4 mm $year^{-1}$ estimated by TEM-AL1. In contrast, the PM-Mu *ET* estimates by Vinukollu et al. (2011) are substantially lower than the other *ET* estimates in NE (Fig. 1), which is consistent with the evaluation by Vinukollu et al. (2011) that showed a sizeable negative bias in that product. The high TEM-AL1 *ET* estimates is mainly due to the overestimation of *ET* in summer months (the difference between TEM-AL1 *ET* and TEM-AL2 *ET* decreases from 28.4 to 9.5 % when *ET* from JJA is not considered). The spatial distribution of TEM-AL2 *ET* matches well with that of GLEAM, EVAL and MODIS-ET (Fig. 1), with r values ranging from 0.79 to 0.92 (Fig. S6).

The seasonal variability of TEM-AL2 *ET* shows good agreement with EVAL and GLEAM (Fig. S7), as reflected by the RMSD (4.7 mm mon^{-1} for EVAL, 5.77 mm mon^{-1} for GLEAM) and the MPD during the growing season (May-Sep., 8.71 % for EVAL, 10.73 % for GLEAM). TEM-AL1 *ET* and PM-Mu *ET* show different seasonality's from TEM-AL2 ET (Table S6). With respect to TEM-AL1 *ET*, the difference is primarily due to the above-mentioned overestimation of *ET* in summer. In the case of PM-Mu-ET, the difference is most likely due to the large negative bias in summer as indicated by Vinukollu et al. (2011).

The general agreement between the calibrated TEM-AL2 *ET* and the *ET* estimates from satellite-based products provides extra confidence in the ability of TEM-AL2 to estimate spatial and temporal variations in *ET* across NE. In the following sections, TEM-AL2 is used to examine how recent

changes in climate in NE have influenced *ET*, water availability (*P-ET*) and river discharge in NE between 1948 and 2009.

3 Results

3.1 Variation of ET in NE for 1948–2009

The *ET* varies greatly among uplands, wetlands and water bodies. The highest *ET* rates occur in water bodies (776–802 mm year^{-1}), followed by wetlands (241–281 mm year^{-1}) and uplands (231–267 mm year^{-1}). The variation of *ET* among land covers is not just caused by the different algorithms and parameters used to estimate *ET* for each cover type or moisture supply, but also differences in climatic conditions. The mean incoming solar radiation (*R*) for water bodies is estimated as 29.37 W m^{-2} higher than for uplands and 48.66 W m^{-2} higher than for wetlands. The mean annual *T* experienced over water bodies is about 4 °C higher than for uplands and 9 °C higher than for wetlands, while the mean *VPD* for water bodies is 2.83 hPa higher than for uplands and 3.81 hPa higher than for wetlands. These differences in climatic conditions occur because most water bodies are located in the southern edge of NE (Fig. S1d) whereas most wetlands are located in the northern parts of NE (Fig. S1c). In addition, the albedo of water bodies is also lower than that of uplands (see Shuttleworth 1992), which leads to more available energy for evaporation. These climatic differences, the unlimited availability of water and the use of different *ET* algorithms for open-water evaporation (see Section 1 and Table S1 in the Supplementary Materials) explain why the *ET* from water bodies is ~3 times that of uplands and wetlands. These open-water *ET* estimates are comparable to previous estimates from the adjacent Caspian Sea and Black Sea (Froehlich 2000; Romanou et al. 2010). On the other hand, the difference in *ET* between uplands and wetlands is small, due to the positive effects on *ET* of a larger *T* and *R* in uplands being offset by the constraint of soil-water limitations.

Within the uplands, *ET* varies among the different plant functional types (Fig. S8): temperate coniferous forests (402.8 mm year^{-1}), temperate deciduous forests (388.9 mm year^{-1}), grasslands (289.6 mm year^{-1}), xeric woodlands (276.8 mm year^{-1}), boreal forest (232.2 mm year^{-1}), wet tundra (187.2 mm year^{-1}), xeric shrublands (175.9 mm year^{-1}) and alpine tundra/polar desert (129.8 mm year^{-1}). Again, this is largely explained by the differences in climate experienced by the different PFTs (Table S7), with higher *ET* in areas of higher energy (i.e., *R*, *T*) and moisture supply (i.e., *P*). While *ET* in the northern NE is mainly limited by energy, *ET* in the southern NE seems more constrained by moisture supply. For example, xeric shrublands in the southern landscapes receive large amounts of energy (high *T* and *R*), but low *P* such that *ET* is limited by moisture availability. In contrast, alpine tundra/polar deserts receive relatively more *P*, but small amount of energy (low *T* and *R*) such that *ET* is mainly limited by energy.

The (area-weighted) ET_a over NE presents a small increasing trend of 0.13 mm year^{-1} ($p<0.05$) from 1948 to 2009 (Fig. 2). The average ET_a/P ratio of 63.6 % is comparable to global ratios reported in previous studies (e.g., Vörösmarty et al. 1998; Miralles et al. 2011a). All three land covers show small but statistically significant ($p<0.05$) positive trends in *ET* (0.09 mm year^{-1} for uplands, 0.26 mm year^{-1} for wetlands and 0.12 mm year^{-1} for water bodies). These changes are consistent with the slight increases in *T* over this period ($p<0.05$): 0.03 °C year^{-1} for the uplands, 0.02 °C year^{-1} for the wetlands and 0.03 °C year^{-1} for the water bodies. No significant trends were detected for *P*, *R* and *C*. The increase in *T* leads to an

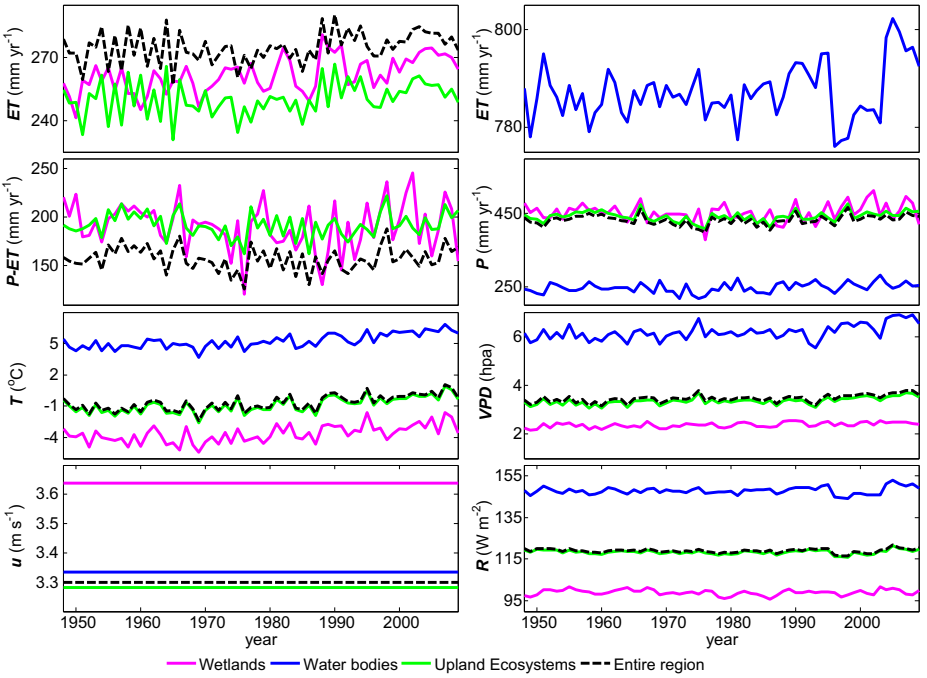

Fig. 2 Inter-annual variability of *ET*, *P–ET* and selected climate variables for the entire NE region, and for the various land covers (uplands, wetlands and water bodies) within NE

increase in vapor pressure deficit (*VPD*, Fig. 2), also an increase in the slope of saturation vapor pressure curve (Δ), a decrease in aerodynamic resistance by promoting turbulences in the surface layer, and a decrease in the stomata resistance by elevating the minimum air temperature. All these processes are accounted for in our representation of *ET* in TEM-AL2 (see Section 1 in the Supplementary Materials). These temperature-related changes result in an increase of *ET*. The *ET* increased for all PFTs in the NE domain – except for xeric woodlands. Boreal forests are the main contributor to *ET* increase due to the largest area percentage (30.8 %) and the highest increasing trend (0.15 mm year^{-1} year^{-1}).

Across NE, the general spatial pattern of ET_a does not change significantly over time (Fig. 3a). The ET_a gradient from the north to mid-latitudes of the domain is almost unchanged from the 1950s to 2000s, with the highest ET_a in the southwest, the southeast and the south-central, where temperate forests and water bodies are abundant. In contrast, although magnitudes of local temporal changes in ET_a (i.e. ΔET_a) are small relative to ET_a, the spatial pattern of ΔET_a differs across the region (Fig. 3b). The large increases of ET_a in the southwest and the large decreases of ET_a in the southeast are consistent with the corresponding changes of precipitation in these areas (also see John et al. 2013). Meanwhile, ET_a presents an overall increasing trend across the NE except the south and north central part (Fig. S9). The trend pattern of ET_a generally matches well with that of *T* and *P*, and it is a consequence of trade-off between individual effects of climate variables (e.g., *P*, *T*, *R* and *VPD*) on ET_a. For example, in the southeast, where *P* is declining and *T* is increasing, ET_a presents a declining trend as the negative effects of limited water supply on ET_a overshadows the promotion of ET_a by warming.

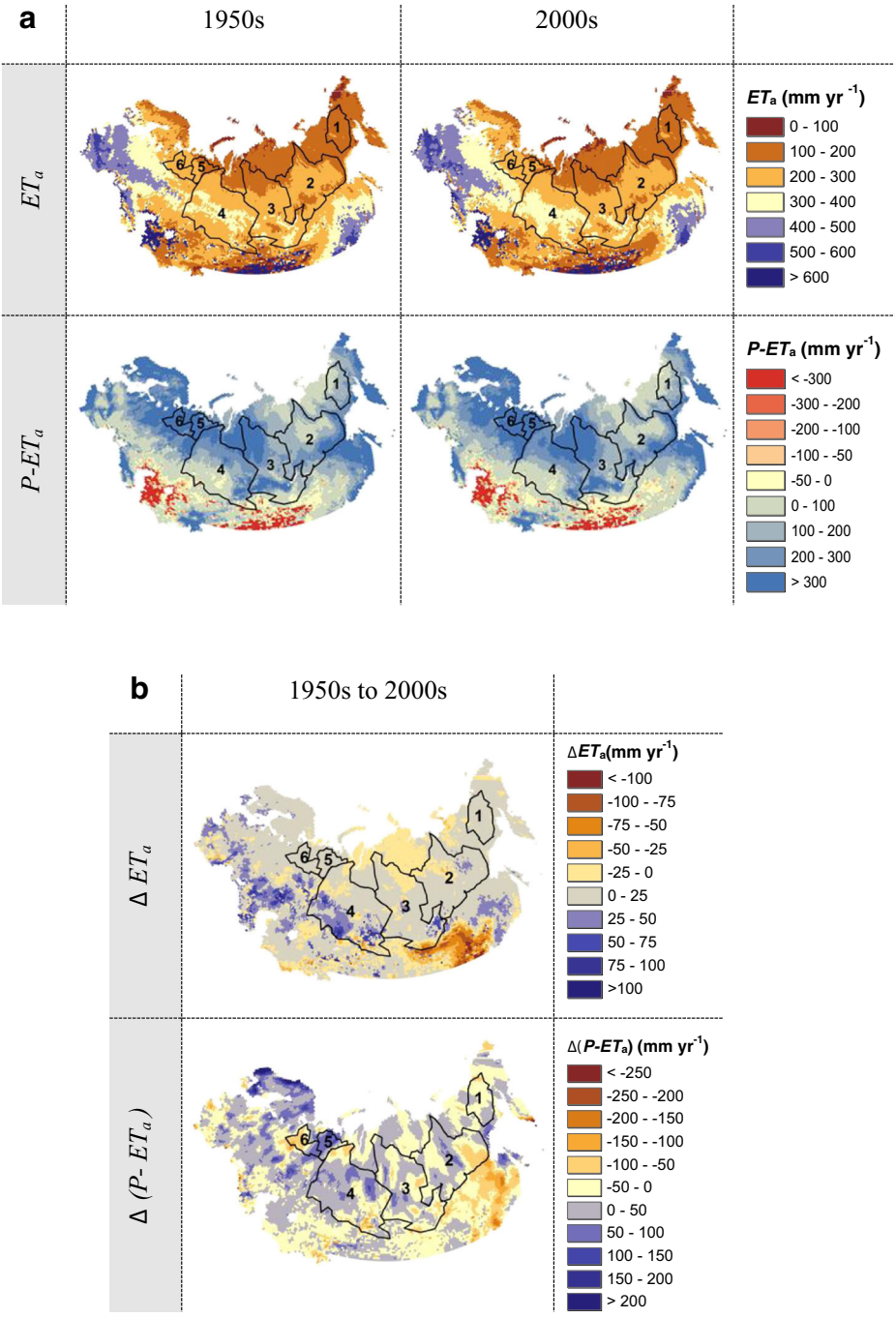

Fig. 3 Average spatial patterns for (**a**) the aggregated *ET* (i.e. ET_a) and $P–ET_a$ in the 1950s and the 2000s, and (**b**) change of ET_a (i.e., Δ ET_a) and change of $P–ET_a$ (i.e., Δ($P–ET_a$)) from the 1950s to the 2000s

3.2 Implications of ET variation for water availability

Changes in *ET* over time and space may lead to a regional intensification or weakening of the water cycle (Huntington 2006; Bates et al. 2008), with direct implications for the recycling of precipitation, generation of runoff and ground water recharge. Overall, $P–ET_a$ in the southern part is lower than that in the north (Fig. 3a), as P is lower and ET_a rates are larger due to warmer climate conditions and more radiation in the south.

Changes in $P–ET_a$ (i.e. $\Delta(P–ET_a)$) for 1948–1999 vary across the NE domain (Fig. 3b), but no significant trends ($p>0.05$) are identified for the entire domain (Fig. 2). The western part of the domain experiences a mild increase in $P–ET_a$ whereas negative trends occur in the east. These results are consistent with observational studies that the climatic conditions in the western part of the high latitudinal NE domain became more humid during the 20th century, whereas drier weather conditions prevailed east of the Ural Mountains (Groisman et al. 2010; John et al. 2013). The opposite trends in $P–ET_a$ in the eastern and the western parts of the region offset each other, such that there is no significant trend in the regional water availability over the study period. However, the spatial pattern of $P–ET_a$ remains nearly unchanged from the 1950s through the 2000s.

Changes in water availability are related to changes in runoff and river discharge. Our simulations indicate that the annual mean volumetric soil moisture varied little from year to year in the NE and does not show a significant long-term trend. These changes in soil water storage over the long periods of this study are insignificant compared to the volumes of P and ET_a. As subsurface flow out of the NE watersheds is also considered to be negligible, then most of the available water will runoff from the watershed and contribute to river discharge. TEM-AL2 estimates of $P–ET_a$ are analyzed for the six largest river watersheds in NE: Kolyma, Lena, Yenisei, Ob, Pechora and Northern Dvina (Fig. 1). These six Eurasian arctic rivers drain about two-thirds of the Eurasian arctic landmass (Peterson et al. 2002). The runoff for each watershed is estimated by aggregating the grid cell level estimates of $P–ET_a$ across the watershed area. Subsequently, runoff estimates from the six watersheds are aggregated to obtain the total river discharge for the six watersheds for the period 1948–1999. Aggregated values are compared to river discharge gauge measurements from the Global Runoff Data Centre (GRDC) and those by Peterson et al. (2002).

The estimates of aggregated river discharge for the six largest watersheds in NE from TEM-AL2 are much closer to the aggregated discharge measurements from the GRDC and Peterson et al. (2002) than those from TEM-AL1 (Fig. 4). Taking the mean discharge from the GRDC and Peterson et al. (2002) as reference, the errors associated with TEM-AL2 (RMSD= 126.23 km^3 $years^{-1}$, MPD=−4.02 %) are much lower than those of TEM-AL1 (RMSD= 527.74 km^3 $years^{-1}$, MPD=−28.5 %). Most of the underestimation of discharge by TEM-AL1 has to do with the overestimation of TEM-AL1 *ET* (Section 2.5). Therefore, improvements in the estimation of *ET* by TEM-AL2 also lead to more realistic estimates of long-term river discharge.

To better understand why TEM-AL2 substantially outperforms TEM-AL1, we conducted a simulation experiment using four grid cells that represent all possible land cover compositions in the NE (Table S8). These four grid cells at quite different locations across NE have been randomly chosen (Fig. 1a). Three grid cells are dominated by either uplands, wetlands, or water bodies, respectively, and the fourth grid cell has mixed land cover types. For each grid cell, we conduct a TEM-AL1 simulation and five TEM-AL2 simulations assuming different land cover compositions and snow scenarios: 1) the prescribed fraction coverage of uplands, wetlands and water bodies in the cell with snow dynamics; 2) the same prescribed fraction coverage as 1) but assuming no snow; 3) assuming 100 % uplands without snow; 4) assuming

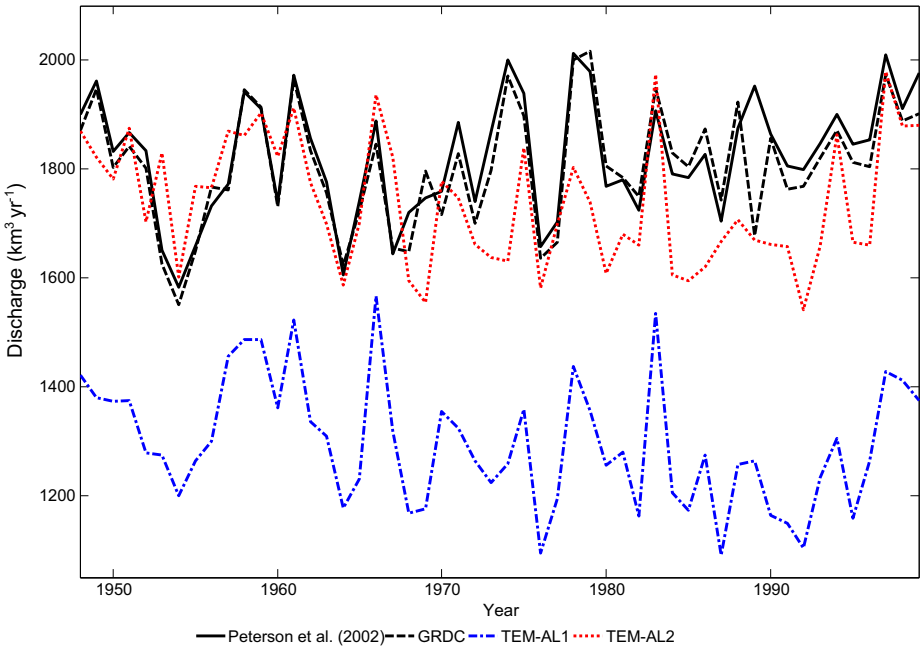

Fig. 4 Discharge from the six largest watersheds in the NE during 1948–1999 as estimated by TEM and previous studies

100 % wetlands without snow; and 5) assuming 100 % water bodies without snow. The *ET* estimates from these 5 scenarios are hereafter referred to as ET_a, ET_{a0}, ET_{u0}, ET_{t0} and ET_{w0}, respectively, to be consistent with previous notations. The TEM-AL1 *ET* is much higher than ET_a across all 4 cells. These results indicate that the use of the Penman-Monteith based equation that has been calibrated to various land cover characteristics in the region will estimate a lower ET, more available water and consequently a higher runoff than the Jensen-Haise formulation. Moreover, ET_a is systematically lower than ET_{a0} across the 4 cells. Consequently, $P–ET_a$ will be much higher and more runoff will occur. This highlights the role of snow on limiting *ET* in the NE region. In addition, differences among ET_{u0}, ET_{t0} and ET_{w0} in each grid cell emphasize the effects of land cover heterogeneity on *ET* estimation and imply that the omission of wetlands and water bodies might cause *ET* to be underestimated in NE.

The estimation of *ET* and runoff in NE has been substantially improved by taking into consideration the influence of land cover characteristics and heterogeneity on AED and *ET*. Most current *ET* estimation schemes, however, do not explicitly consider the detailed *ET* processes examined in this study (Mengelkamp et al. 2006; Mueller et al. 2013) and may lead to large bias in *ET* and runoff. This is especially significant for the NE region as snow, wetlands and water bodies play important roles in the hydrological processes (Arctic Climate Impact Assessment ACIA 2005). Although snow sublimation accounts for a small portion of the total *ET* (mostly<8 %, Fig. S10), consideration of snow dynamics limits the magnitude of total *ET* and improves the realism of *ET* representation in NE where snow prevails during several months in a year.

Unlike previous studies (e.g., Groisman et al. 2010; Peterson et al. 2002), no significantly positive trends in river discharge in the NE have been simulated by the TEM. The consistent underestimation of aggregated discharge after 1970 implies that there might be some other water sources or water dynamics that increase river discharge that are not being considered,

such as the melting of glaciers, the thawing of permafrost, inter-basin transfer, land-use change and fire disturbances (Adam et al. 2007; 2008). In addition, biases in *ET* estimation will also lead to systematic biases in estimating river discharge. Our *ET* estimation may be biased by the lack of consideration of CO_2 effects on stomata conductance, the use of a seasonal climatology for wind speed and snow cover, the assumption of unlimited water supply for *ET* in wetlands, and the assumption of a constant land cover.

4 Conclusions

The *ET* response to the changing climate in the NE and its implications for water availability and river discharge from 1948 through 2009 have been explored using an improved version of the TEM that incorporates more *ET* processes (i.e., canopy interception loss, evaporation from wet land surfaces, evaporation from water bodies and wetlands, and snow sublimation) and considers the influence of a heterogeneous land cover on *ET*. Comparisons of model results to in situ measurements of *ET* and satellite products demonstrate that the improved algorithms captures the spatiotemporal changes of *ET* in NE substantially better than the previous version of TEM, which did not consider the influence of land characteristics on atmospheric evaporative demand (AED). Our results suggest that *ET* has increased during our study period as a consequence of the concurrent slight rise in air temperature.

Improvements in the estimation of *ET* have caused more water to be available for runoff, which has also led to improvements in model estimates of river discharge. These improvements mainly result from a reduced AED estimate by the new algorithms and the influence of snow cover on limiting *ET*. Consideration of wetlands and water bodies in the landscape leads to higher *ET* estimates in the NE than if the presence of these wet land covers is ignored. Finally, our analyses indicate that latent heat fluxes measured at eddy-covariance flux sites provide useful information for improving the simulation of regional hydrometeorology by land surface models.

Acknowledgments This research is supported by the NASA Land Use and Land Cover Change program (NASA- NNX09AI26G, NN-H-04-Z-YS-005-N, and NNX09AM55G), the Department of Energy (DE-FG02-08ER64599), the National Science Foundation (NSF-1028291 and NSF- 0919331), the NSF Carbon and Water in the Earth Program (NSF-0630319), and the Dynamics of Coupled Natural and Human Systems (CNH) Program of the NSF (#1313761).. We also acknowledge the Global Runoff Data Centre for provision of the gauge station data. Runoff data in Peterson et al. (2002) were obtained from the R-ArcticNet database. A special acknowledgment is made here to Prof. Eric Wood for his generous provision of the ET datasets of Vinukollu et al. (2011), and to Dr. Brigitte Mueller and Dr. Martin Hirsci for the provision of the LandFlux-EVAL dataset of Mueller et al. (2013). Diego Miralles acknowledges the support by the European Space Agency WACMOS-ET project (4000106711/12/I-NB).

References

Adam JC, Lettenmaier DP (2008) Application of New precipitation and reconstructed discharge products to discharge trend attribution in Northern Eurasia. J Clim 21(8):1807–1828

Adam JC, Haddeland I, Su F, Lettenmaier DP (2007) Simulation of reservoir influences on annual and seasonal discharge changes for the Lena, Yenisei, and Ob'rivers. J Geophys Res Atmos 112:D24 (1984–2012)

Arctic Climate Impact Assessment (ACIA) (2005) Cambridge University Press, New York, p 1042

ASCE (American Society of Civil Engineers) (1996) Hydrology handbook. ASCE manuals and reports on engineering practice No. 28. ASCE, New York

Bates B, Kundzewicz ZW, Wu S, Palutikof J (2008) IPCC: Climate change and water

Dolman AJ, De Jeu R (2010) Evaporation in focus. Nat Geosci 3(5):296–296

Dorigo WJR, Chung D, Parinussa R, Liu Y, Wagner W, Fernández-Prieto D (2012) Evaluating global trends (1988–2010) in harmonized multi-satellite surface soil moisture. Geophys Res Lett 39:18
Douville H, Ribes A, Decharme B, Alkama R, Sheffield J (2012) Anthropogenic influence on multidecadal changes in reconstructed global evapotranspiration. Nat Clim Chang 3:59–62
Feddes RA, Lenselink KJ (1994) Evapotranspiration. In: H.P. Ritzema (ed) Drainage principles and applications. Water Resources Pubns, Wageningen, The Netherlands, p 1125
Fisher JB, Tu KP, Baldocchi DD (2008) Global estimates of the land–atmosphere water flux based on monthly AVHRR and ISLSCP-II data, validated at 16 FLUXNET sites. Remote Sens Environ 112(3):901–919
Frey KE, Smith LC (2003) Recent temperature and precipitation increase in West Sibria and their association with the Arctic Oscillation. Polar Res 22(2):287–300
Froehlich K (2000) Evaluating the water balance of inland seas using isotopic tracers: the Caspian Sea experience. Hydrol Process 14(8):1371–1383
Groisman PY, Clark EA, Kattsov VM, Lettenmaier DP et al (2009) The Northern Eurasia earth science partnership: an example of science applied to societal needs. Bull Am Meteorol Soc 5:671–688
Groisman P, Gutman G, Reissell A (2010) Introduction: climate and land-cover changes in the arctic. In: Gutman G, Reissell A (eds) Eurasian arctic land cover and land use in a changing climate. Springer, London, pp 1–8
Hamed KH, Rao AR (1998) A modified Mann–Kendall trend test for autocorrelated data. J Hydrol 204:182–196
Harris I, Jones P, Osborn T, Lister D (2013) Updated high-resolution grids of monthly climatic observations–the CRU TS3. 10 dataset. Int J Climatol. doi:10.1002/joc.3711
Held IM, Soden BJ (2000) Water vapor feedback and global warming. Annu Rev Energy Environ 25:441–475
Huntington TG (2006) Evidence for intensification of the global water cycle: review and synthesis. J Hydrocarb 319(1):83–95
IPCC (2013) Climate change 2013: the physical science basis. Working Group I Contribution to the Fifth Assessment Report of the Intergovernmental Panel on Climate Change, Summary for Policymakers, IPCC
Jensen ME, Haise HR (1963) Estimating evapotranspiration from solar radiation, Proceedings of the American Society of Civil Engineers. J Irr Drain Div 89:15–41
Jin Y, Schaaf CB, Woodcock CE, Gao F, Li X, Strahler AH, Lucht W, Liang S (2003a) Consistency of MODIS surface bidirectional reflectance distribution function and albedo retrievals: 1. Algorithm performance. J Geophys Res 108(D5)
Jin Y, Schaaf CB, Woodcock CE, Gao F, Li X, Strahler AH, Lucht W, Liang S, (2003b) Consistency of MODIS surface bidirectional reflectance distribution function and albedo retrievals: 2. Validation J Geophys Res 108(D5)
John R et al (2013) Vegetation response to extreme climate events on the Mongolian Plateau from 2000–2010. Environ Res Lett 8:035033
Jung M et al (2010) Recent decline in the global land evapotranspiration trend due to limited moisture supply. Nature 467(7318):951–954
Kumar S, Lawrence DM, Dirmeyer PA, Sheffield J (2014) Less reliable water availability in the 21st century climate projections. Earth's Futur 2:152–160
Liu Y, Zhuang Q, Chen M, Tchebakova N, Pan Z et al (2013) Response of evapotranspiration and water availability to changing climate and land cover on the Mongolian Plateau during the 21st century. Global Planet Chang 108:85–99
McClelland JW, Holmes RM, Peterson BJ, Stieglitz M (2004) Increasing river discharge in the Eurasian Arctic: consideration of dams, permafrost thaw, and fires as potential agents of change. J Geophys Res-Atmos 109: D18 (1984–2012)
Mengelkamp H-T et al (2006) Evaporation over a heterogeneous land surface: the EVA-GRIPS project. Bull Am Meteorol Soc 87:775–786
Miralles DG, De Jeu RAM, Gash JH, Holmes TRH, Dolman AJ (2011a) Magnitude and variability of land evaporation and its components at the global scale. Hydrol Earth Syst Sci 15(3):967–981
Miralles DG, De Jeu RAM, Gash JH, Holmes TRH, Dolman AJ (2011b) Global land-surface evaporation estimated from satellite-based observations. Hydrol Earth Syst Sci 15(2):453–469
Mohamed YA, Bastiaanssen WGM, Savenije HHG, van den Hurk BJJM, Finlayson CM (2012) Wetland versus open water evaporation: an analysis and literature review. Phys Chem Earth 47–48:114–121
Monteith JL (1965) Evaporation and environment. Symp Soc Exp Biol 19:205–224
Mu Q, Zhao M, Running SW (2011) Improvements to a MODIS global terrestrial evapotranspiration algorithm. Remote Sens Environ 115(8):1781–1800
Mueller B et al (2013) Benchmark products for land evapotranspiration: LandFlux-EVAL multi-dataset synthesis. Hydrol Earth Syst Sci 17:3707–3720
NEESPI (2004) The Northern Eurasia Earth Science Partnership Initiative (NEESPI), Executive Overview

Pan Y, Mcguire AD, Kicklighter DW, Melillo JM (1996) The importance of climate and soils for estimates of net primary production: a sensitivity analysis with the terrestrial ecosystem model. Glob Change Biol 2(1):5–23
Penman HL (1948) Natural evaporation from open water, bare soil and grass. Proceedings of the Royal Society of London, Series A Mathematical and Physical Sciences 193(1032):120–145
Penman HL (1956) Evaporation: an introductory survey. Neth J Agr Sci 4(1):9–29
Peterson BJ et al (2002) Increasing river discharge to the Arctic Ocean. Science 298(5601):2171–2173
Romanou A, Tselioudis G, Zerefos CS, Clayson CA, Curry JA, Andersson A (2010) Evaporation-precipitation variability over the Mediterranean and the Black Seas from satellite and reanalysis estimates. J Clim 23(19): 5268–5287
Salomon J, Schaaf CB, Strahler AH, Gao, F, Jin Y (2006) Validation of the MODIS bidirectional reflectance distribution function and albedo retrievals using combined observations from the aqua and terra platforms. IEEE Trans Geosci Remote Sens 44(6):1555–1565
Seneviratne SI et al (2010) Investigating soil moisture–climate interactions in a changing climate: a review. Earth Sci Rev 99:125–161
Shuttleworth WJ (1992) Evaporation. In: Maidment DR (ed) Handbook of hydrology. McGraw Hill, New York
Simmons A et al (2004) Comparison of trends and low-frequency variability in CRU, ERA-40, and NCEP/ NCAR analyses of surface air temperature. J Geophys Res Atmos 1984–2012:109
Stephens GL et al (2012) An update on Earth's energy balance in light of the latest global observations. Nat Geosci 5:691–696
Vinukollu RK, Wood EF, Ferguson CR, Fisher JB (2011) Global estimates of evapotranspiration for climate studies using multi-sensor remote sensing data: evaluation of three process-based approaches. Remote Sens Environ 115(3):801–823
Vörösmarty CJ, Federer CA, Schloss AL (1998) Potential evaporation functions compared on U.S. watersheds: possible implications for global-scale water balance and terrestrial ecosystem modeling. J Hydrol 207(3–4): 147–169
Vörösmarty CJ et al (2010) Global threats to human water security and river biodiversity. Nature 467(7315):555–561
Wang K, Dickinson RE (2012) A review of global terrestrial evapotranspiration: observation, modeling, climatology, and climatic variability. Rev Geophys 50:RG2005
Xiao J, Chen J, Davis KJ, Reichstein M (2012) Advances in upscaling of eddy covariance measurements of carbon and water fluxes. J Geophys Res 117:G00J01
Zhang P (1993) Model selection via multifold cross validation. Ann Stat 21(1):299–313
Zhuang Q, McGuire, AD, O'Neill KP, Harden JW, Romanovsky VE, Yarie J (2002) Modeling soil thermal and carbon dynamics of a fire chronosequence in interior Alaska. J Geophys Res 108
Zhuang Q, He J, Lu Y, Ji L, Xiao J, Luo T (2010) Carbon dynamics of terrestrial ecosystems on the Tibetan Plateau during the 20th century: an analysis with a process-based biogeochemical model. Glob Ecol Biogeogr 19(5):649–662